European Journal of Cancer 176 (2022) 41–49

Available online at www.sciencedirect.com

ScienceDirect

journal homepage: www.ejcancer.com

Original Research

DeepClassPathway: Molecular pathway aware classification using explainable deep learning

Elia Lombardo [a,1], Julia Hess [a,b,c,1], Christopher Kurz [a], Marco Riboldi [d], Sebastian Marschner [a], Philipp Baumeister [b,e], Kirsten Lauber [a,c], Ulrike Pflugradt [a,c], Axel Walch [d,f], Martin Canis [b,e], Frederick Klauschen [g,h], Horst Zitzelsberger [a,b,c], Claus Belka [a,c,h], Guillaume Landry [a,2], Kristian Unger [a,b,c,*,2]

[a] *Department of Radiation Oncology, University Hospital, LMU Munich, Munich, 81377, Germany*
[b] *Research Unit Radiation Cytogenetics, Helmholtz Zentrum München, German Research Center for Environmental Health GmbH, Neuherberg, Germany*
[c] *Clinical Cooperation Group "Personalized Radiotherapy in Head and Neck Cancer", Helmholtz Zentrum München, German Research Center for Environmental Health GmbH, Neuherberg, Germany*
[d] *Department of Medical Physics, Faculty of Physics, Ludwig-Maximilians-Universität München, Garching, 85748, Germany*
[e] *Department of Otorhinolaryngology, Head and Neck Surgery, University Hospital, LMU Munich, Munich, 81377, Germany*
[f] *Research Unit Analytical Pathology, Helmholtz Zentrum München, German Research Center for Environmental Health GmbH, Neuherberg, Germany*
[g] *Institute of Pathology, Faculty of Medicine, Ludwig-Maximilians-University of Munich, Munich, Germany*
[h] *German Cancer Consortium (DKTK), Partner Site Munich, Munich, 81377, Germany*

Received 7 July 2022; accepted 25 August 2022
Available online 30 September 2022

KEYWORDS
HNSCC;
HPV;
Transcriptome;
Deep learning;
CNN;
Grad-CAM

Abstract ***Objective:*** HPV-associated head and neck cancer is correlated with favorable prognosis; however, its underlying biology is not fully understood. We propose an explainable convolutional neural network (CNN) classifier, DeepClassPathway, that predicts HPV-status and allows patient-specific identification of molecular pathways driving classifier decisions.
Methods: The CNN was trained to classify HPV-status on transcriptome data from 264 (13% HPV-positive) and tested on 85 (25% HPV-positive) head and neck squamous carcinoma patients after transformation into 2D-treemaps representing molecular pathways. Grad-CAM saliency was used to quantify pathways contribution to individual CNN decisions. Model stability was assessed by shuffling pathways within 2D-images.
Results: The classification performance of the CNN-ensembles achieved ROC-AUC/PR-AUC

* *Corresponding author*: Department of Radiation Oncology, University Hospital, LMU Munich, Munich, 81377, Germany.
E-mail address: unger@helmholtz-muenchen.de (K. Unger).
[1] Contributed equally as lead author. [2] Contributed equally as senior author.

https://doi.org/10.1016/j.ejca.2022.08.033

of 0.96/0.90 for all treemap variants. Quantification of the averaged pathway saliency heatmaps consistently identified KRAS, spermatogenesis, bile acid metabolism, and inflammation signaling pathways as the four most informative for classifying HPV-positive patients and MYC targets, epithelial–mesenchymal transition, and protein secretion pathways for HPV-negative patients.

Conclusion: We have developed and applied an explainable CNN classification approach to transcriptome data from an oncology cohort with typical sample size that allows classification while accounting for the importance of molecular pathways in individual-level decisions.

1. Introduction

One of the main applications of cancer omics is the prediction of prognostically relevant disease subentities. Many transcriptome-based classifiers predicting clinical outcome or defining transcriptional subtypes have been published in recent years, with most studies using a regression-based machine learning methodology [1]. Regression models come with the advantage of low complexity, which can be beneficial, but limits biological explainability. Deep learning with neural networks can make use of the full complexity of a dataset and allows reconstruction of the information used in decision making with explainable artificial intelligence methods.

Strategies for using omics- and gene expression data as input to neural networks range from using them directly as gene expression vectors, representation vectors resulting from encoding/decoding or graph convolutional neural networks after mapping gene expressions to protein–protein interaction (PPi) networks [2]. However, these strategies do not sufficiently allow post hoc reconstruction of the biological information important for neural network decision making. One promising approach for overcoming this is to organize the gene expression into 2D-images with a structured representation of molecular pathways. Lopez-Garcia *et al.* (2020) first applied this concept by organizing gene expression into pathway 2D-treemaps as input for convolutional neural network (CNNs) predicting clinical outcome in a pan-cancer study [3]. The resulting model showed good performance, but explainability was not investigated.

High-risk human papilloma virus (HPV)-associated and HPV-negative head and neck squamous cell carcinoma (HNSCC), primarily associated with smoking and alcohol consumption, are regarded as distinct cancer entities which are clearly characterized by different clinical and molecular properties [4–7]. HPV-associated tumors treated with (chemo)radiation therapy have a better clinical prognosis and exhibit different transcriptional profiles compared to HPV-negative tumors. As comprehensive knowledge on the underlying biology of HPV- associated and -negative HNSCC exists and HPV-status typing is well established and robust we considered transcriptome data from HPV-characterized HNSCC as ideal real-world data for the development of an explainable deep learning approach for the prediction of disease.

We developed and present DeepClassPathway, a workflow that transforms transcriptome profiles into 2D-images representing the gene expressions of 50 molecular pathways as an input for training and application of a classification CNN-ensemble (see Fig. 1 for an overview). Our concept was applied to a whole RNA-seq dataset from an in-house HNSCC cohort and a HNSCC cohort from The Cancer Genome Atlas (TCGA) [1,4,8]. The contributions of each molecular pathway to decision making were reconstructed by querying the magnitude of grad-CAM saliency heatmaps at the locations of pathways within the gene expression 2D-image [9].

We describe a reproducible workflow for generating explainable CNN classification models, which can be generally applied to any transcriptome dataset with binary ground truth labels and demonstrate its predictive capabilities and the plausibility of the reconstructed biological information used in the model decision process.

2. Methods

2.1. HNSCC patient cohorts

The TCGA (n = 277) and the LMU-KKG (n = 72, Ludwig-Maximilians-University of Munich, Clinical Cooperation Group 'Personalized Radiotherapy in Head and Neck Cancer') HNSCC cohorts were analyzed [1,4,8]. Clinical patient data from cBioPortal and the TCGA GDC data portal [10,11] were used. The LMU-KKG cohort included patients with HNSCC of the hypopharynx, oropharynx, or oral cavity who had undergone surgical resection followed by adjuvant (chemo)radiotherapy treatment at the Department of Radiation Oncology, LMU University Hospital, Germany, between 2008 and 2013 [8]. This study on clinical and biological data was approved by the local ethics

committee in Munich (EA 448-13 and 17-116) and was carried out in accordance with the Declaration of Helsinki. HPV status for TCGA specimens was from the clinical patient data [4]. HPV status for LMU-KKG specimens was determined as previously reported [12].

The clinical and histopathological data for TCGA and LMU-KKG patients included in the training and testing sets are presented in SI Table 1.

2.2. Transcriptome data preprocessing

A detailed description of transcriptome data preprocessing can be found in the supplementary extended methods section. In brief, the LMU RNA-seq data raw sequencing reads were adapter-trimmed, aligned and counted per gene. Raw counts of the TCGA cohorts were downloaded from the GDC data portal. All read counts were imported into DESeq2 before calculation of variance stabilization transformed (vst) gene expressions. The resulting vst-value matrix was used as input for generating the 2D-treemap images.

2.3. Transformation of gene expressions into 2D-treemap images

In a first step the gene expression vector (vst) of each patient was assigned to the genes defining each of the 50 MsigDB pathways and the resulting data frame was converted to 500 × 500 pixels treemaps. Each gene within the rectangles gets a greyscale value according to its gene expression value (high expression: dark, low expression: light). The MsigDB Hallmark genes have been selected because they contain only ground-truth evaluated genes [13]. As all 50 Hallmark pathways are contained, each 2D-image represents the molecular biological makeup of each tumor. To evaluate the robustness of our approach we generated three different variants of treemaps, leading to three different permutations of the pathway locations in the treemaps and optimized the CNN models separately for each one of the treemap variants.

2.4. Deep learning model

We implemented a 2D-CNN [14,15] with three convolutional blocks and 3 × 3 kernels for binary classification of HPV status. A detailed description of the 2D-CNN architecture can be found in the supplementary extended methods section.

2.5. Model optimization and details

We trained the model using cross-validation on the training dataset, which was built by randomly selecting about 75% of the patients from the combined cohorts, with the remainder used as testing set. The training patients were subsequently split to perform 3-fold cross validation. This procedure was repeated 10 times with random initialization, thus 30 different CNN models were trained and validated. The models were then applied to the testing data and by averaging the predicted probabilities over the models, we obtained for every patient a probability for HPV-positive and HPV-negative. All models were trained using the categorical cross entropy loss function and the Adam optimizer. Weight decay was used additionally to dropout as regularization technique [16]. The hyper-parameters found to perform best are shown in Table 1.

2.6. Pathway saliency mapping

To determine which pathways of the treemaps are related to HPV status, we used the gradient-weighted class activation mapping (grad-CAM) method [[9],18]. It uses the gradients of a predicted class probability with respect to the feature set of the last convolutional layer to produce a coarse saliency map. The saliency maps are subsequently up-sampled to the shape of the input treemap, as can be seen in the bottom left part of Fig. 1. From the up-sampled saliency map, the saliencies of different tumor pathways were calculated by taking the average of the saliency map within all given pathway regions. Saliency maps were calculated separately for patients with clinically proven HPV-positive status with respect to the HPV-positive class and for patients with clinically proven HPV-negative status with respect to the HPV-negative class prediction. We computed pathway saliency only for models that predicted the correct HPV-status with scores higher than 0.70. Finally, the average saliency per pathway obtained for correctly classified patients was averaged over all models. Therefore, we obtained a patient and model averaged saliency per pathway and treemap variant (see Fig. 2).

2.7. Explainability

To visualize the relatedness of MsigDB Hallmark paths, a network graph was drawn, where pathways were represented as nodes and edges were weighted according to the number of overlapping genes between two paths. The Kamada Kawai layout was chosen so that the distance between nodes reflected their relatedness in terms of overlapping genes.

Table 1
Best set of CNN hyper-parameters found using the first treemap variant. The same hyper-parameters were then used for the other two variants.

Hyper-parameter	Best performing value
Learning rate	2×10^{-4}
Weight decay	1×10^{-5}
Dropout rate	0.30
Batch size	32

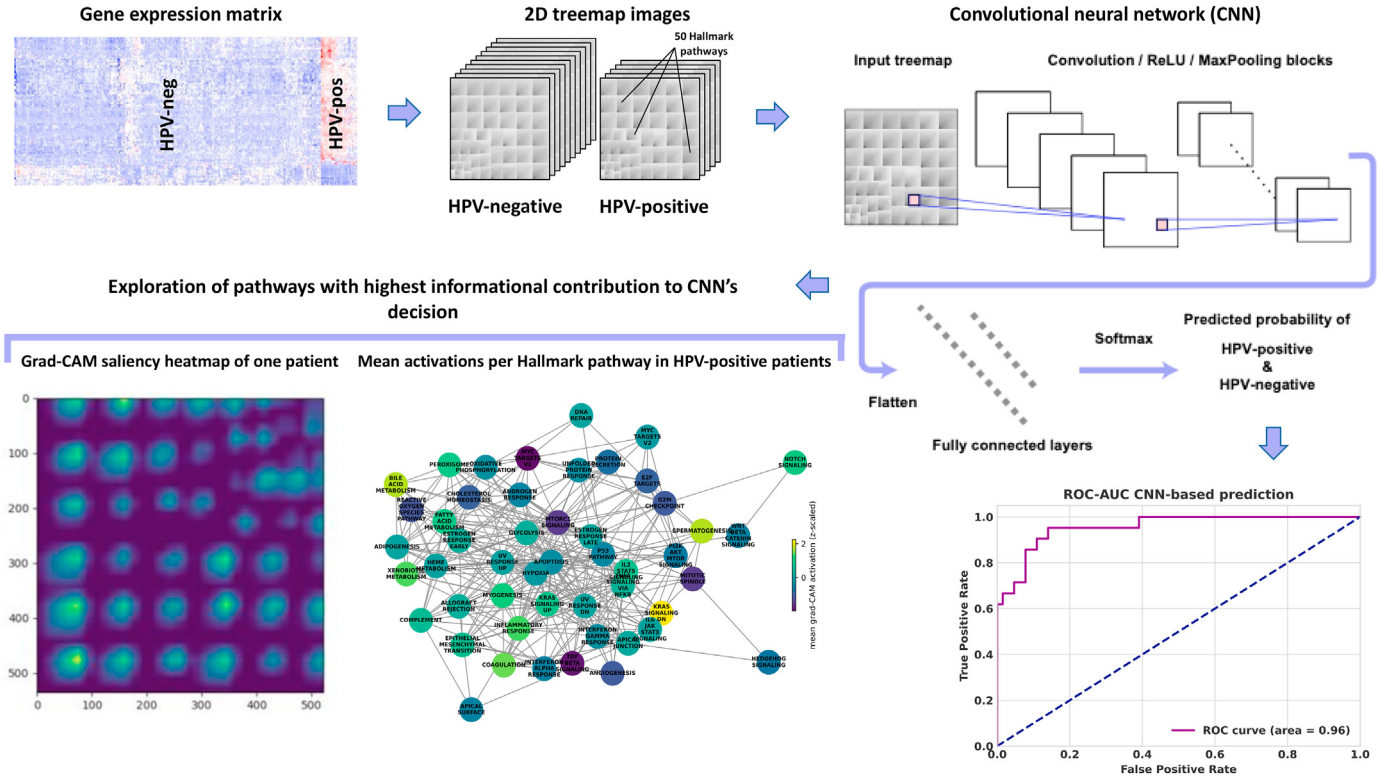

Fig. 1. (color): Workflow of CNN-based prediction of disease subentities using treemap-transformed gene expression data. The upper panel describes the prediction of the HPV-status by a CNN-model using gene expression data transformed into pathway treemaps, followed by performance assessment using ROC-AUC (bottom right) and explainability by grad-CAM saliency mapping to the pathways (bottom left).

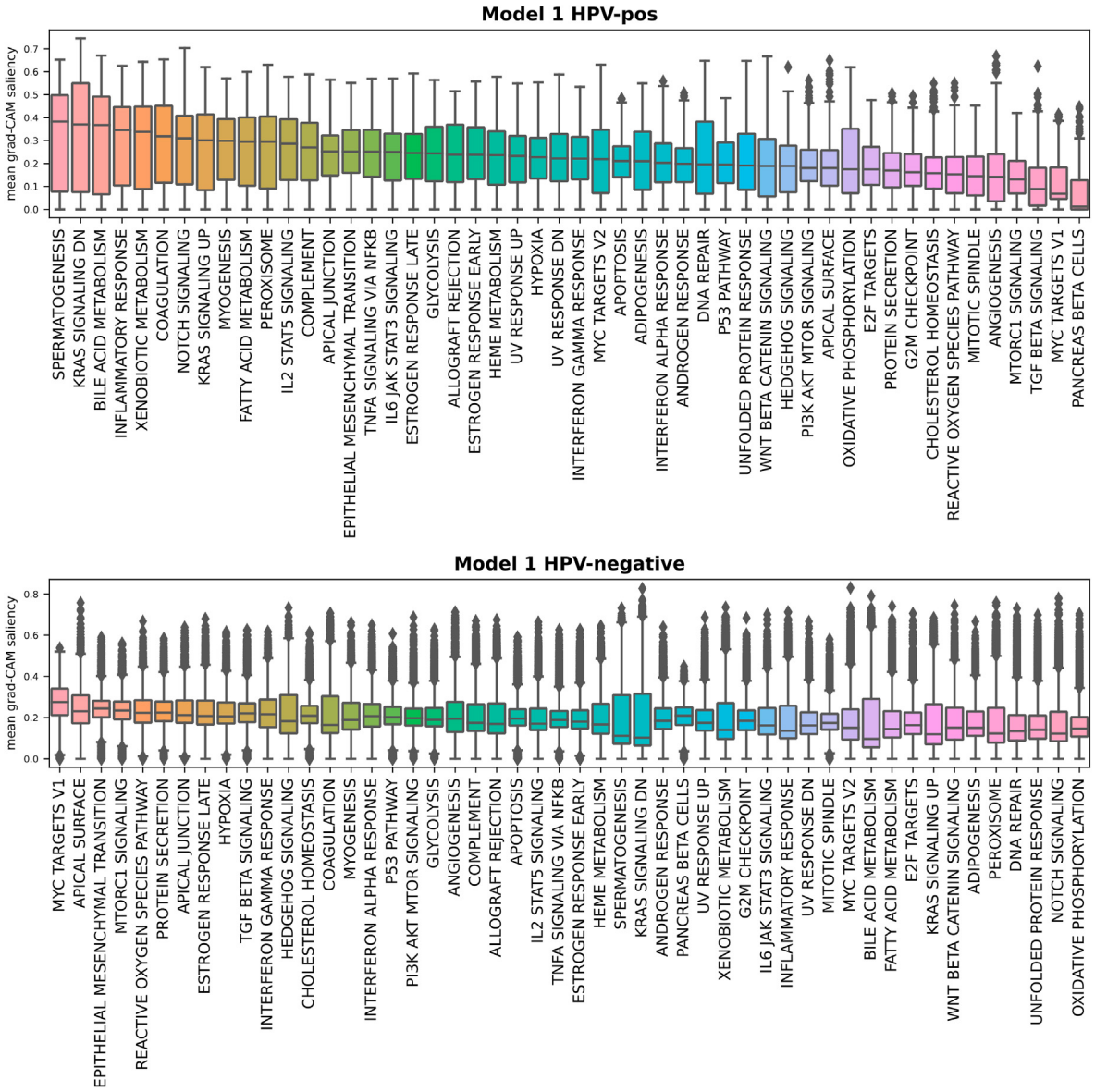

Fig. 2. (color): Mean grad-CAM saliencies obtained from the classification of HPV-positive (top) and HPV-negative (bottom) testing set patients. Shown are boxplots of grad-CAM saliencies averaged across the CNN model ensemble 1, sorted by median order from left to right.

2.8. Predictive power

The discriminative performance in predicting HPV-status was evaluated with the receiver operating characteristics area under the curve (ROC-AUC) [19], and with the precision-recall area under the curve (PR-AUC) for imbalanced datasets [20].

3. Results

3.1. RNA-seq data

After random splitting, the training set (n = 264) contained n = 232 cases from the TCGA and n = 32 cases from the in-house LMU-KKG cohort and the test set (n = 85) consisted of n = 45 patients from the TCGA and n = 40 from the in-house cohort (SI Table 1). In total the dataset contained n = 22,866 genes.

3.2. Explainability

Heatmaps of the grad-CAM saliencies for each patient and model contained in model ensemble 1 can be found in SI File 1 for the prediction of HPV-associated and in SI File 2 for HPV-negative predictions. The top five mean grad-CAM salient MsigDB Hallmark pathways for the prediction of HPV-positive patients were spermatogenesis, KRAS-signaling (down), bile acid metabolism, inflammatory response and xenobiotic metabolism. In HPV-negative patients the most salient

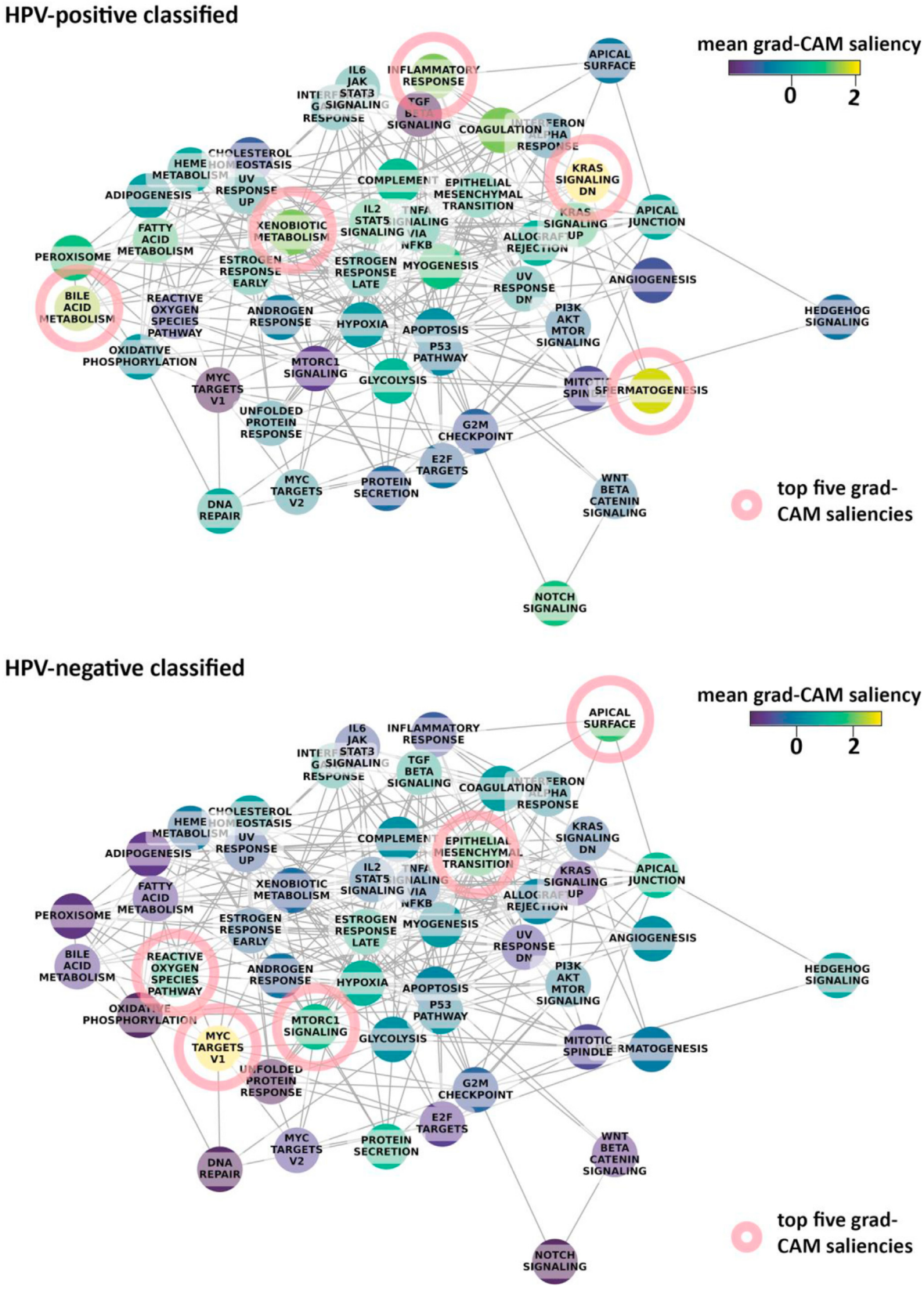

Fig. 3. (color): Hallmark pathway gene overlap network with mapped mean grad-CAM saliencies of HPV-positive (upper panel) and HPV-negative (lower panel) classified testing set patients. Network nodes are Hallmark pathways colored by the grad-CAM saliencies averaged across CNN model ensemble 1 and patients. Edges indicate shared genes between two paths, and the edge length is weighted by the number of shared genes. The closer the network nodes are to each other, the more genes they have in common. The top five salient pathways are indicated by pink circles. (For interpretation of the references to color in this figure legend, the reader is referred to the Web version of this article.)

Table 2
Prediction performance of CNN models for different input treemap variants.

CNN-Model	ROC-AUC test	PR-AUC test
Model ensemble 1	0.955	0.900
Model ensemble 2	0.959	0.904
Model ensemble 3	0.958	0.904

pathways were MYC targets (v1), apical surface, epithelial mesenchymal transition, MTORC1 signaling and reactive oxygen species (Fig. 2). The top salient pathways for both HPV-positive and negative for model ensemble 1, were also found in the top 10 of model ensemble 2 and 3 (SI File 3). The mean pathway saliencies in HPV-negative patients showed higher homogeneity expressed by smaller variation across pathways (SD: 0.017, range: 0.19–0.26) compared to HPV-positive patients (SD: 0.056, range: 0.08–0.34). The distributions of variances of the mean pathway saliencies in both groups were significantly different (Levene's homogeneity test p-value $< 10^{-7}$).

The relatedness of the 50 Hallmark pathways in terms of genes shared between the underlying gene sets is visualized in Fig. 3, with mean grad CAM saliency values assigned to pathway nodes. The five major signaling pathways in HPV-positive predictions, KRAS-signaling (down), spermatogenesis, and inflammatory response pathways form a direct connection subnetwork, as do xenobiotic metabolism and bile acid metabolism. In HPV-negative predictions from the top five salient pathways MYC targets (v1), apical surface, epithelial mesenchymal transition, MTORC1 form a directly connected subnetwork with no direct connection to the reactive oxygen species pathway. In order to identify grad-CAM saliency patterns the mean grad-CAM saliencies per patient and pathway were subjected to unsupervised hierarchical clustering, and four main grad-CAM patterns were found (SI Fig. 2).

3.3. Predictive power

For the three treemap variants and the corresponding ensembles of models, ROC-AUC was 95.5%, 95.9% and 95.8% and PR-AUC was 90.1%, 90.4% and 90.4% (Table 2 and SI Fig. 1).

4. Discussion

In addition to assessing predictive power, which was consistently good across model ensembles, we thoroughly explored the capabilities of our approach with respect to explainability expressed by grad-CAM. Overall, we observed higher homogeneity of pathway mean grad-CAM saliencies in HPV-negative- compared to HPV-positive patients. This goes along with a clear ranking of mean pathway grad-CAM saliencies observed in HPV-positive- but not in HPV-negative-predicted patients. In contrast to HPV-negative HNSCC, tumorigenesis of HPV-related tumors is characterized by deregulated expression of the HPV oncogenes E6 and E7, which inactivate RB and p53, respectively, and lead to immortalization and cancer progression through the accumulation of typical alterations such as PIK3CA mutations or amplifications [6,7]. The process of tumorigenesis in HPV-negative tumors is not triggered by HPV viruses and is therefore rather stochastic, which on average should lead to a more regular distribution of activated pathways as observed in our data. The top five pathway grad-CAM saliencies in HPV-associated predicted patients were spermatogenesis, KRAS signaling, bile acid metabolism, inflammatory response and xenobiotic metabolism. Martinez *et al.* (2007) reported specific upregulation of spermatogenesis genes in HPV-positive HNSCC [21]. Further, it is known that HPV-driven HNSCC regulate the inflammatory response in the frame of immune escape [22]. Only little knowledge is available on disturbed KRAS-signaling in HNSCC—only rare occurrence of KRAS-mutation is reported [23]. Bile acid metabolism and xenobiotic metabolism are not plausible in the context of HNSCC. This can be explained by the unspecific detection of their saliencies due to genes present not only in these but also in other signaling. Hence, improving the specificity of ground truth-based pathway gene sets would be an important next step towards improving their usability. The pathways MYC targets (v1), apical surface, epithelial mesenchymal transition, MTORC1 signaling and reactive oxygen species with highest grad-CAM saliencies in the HPV-negative predicted patients are consistent with published findings on HNSCC and squamous cell carcinogenesis [23–26] and therefore highlight the plausibility of the approach. The pathways which showed highest mean grad-CAM activations showed overall consistent patterns in HPV-associated and HPV-negative patients as identified by hierarchical clustering. Two out of three HPV-associated patients misclassified as HPV-negative by our models showed an overall low grad-CAM activation which is probably due to faulty transcriptomic profiles. The third HPV-associated patient misclassified as HPV-negative and the HPV-associated cases classified as HPV-negative showed grad-CAM patterns which are typical for their predicted class, which could be due to clinical misclassification.

5. Conclusion

In this study, we developed a deep learning model for the prediction of HPV-status from transcriptome data in head and neck cancer patients from two independent cohorts which achieved very good and stable classification performance. The advantage of the proposed CNN model was identified in its biological explainability, as it

provides the molecular pathway information that determined the classification at an individual patient level. In conclusion, we showed that CNNs can be successfully applied to transcriptomic datasets with sample sizes usual in translational clinical science to predict a meaningful endpoint and obtain information about the biological pathways driving the model's prediction. This provides the starting point for the further development of explainable transcriptome-based CNN prediction models.

Data availability

The TCGA HNSC data used in this paper are available from the GDC data legacy portal. RNA-seq data generated from the in-house HNSCC cohort are available from Gene Expression Omnibus under the accession number GSE205308.

Funding

This study was supported by the German Federal Ministry of Education and Research (BMBF) project ZiSStrans (02NUK047A to JH, KU and HZ and 02NUK047C to CB and KL).

Author contributions

Conceptualization, G.L., J.H., and K.U.; methodology, C.K., E.L., G.L., J.H., M.R. and K.U.; software, E.L. and K.U.; validation, C.K., J.H, E.L., G.L., M.R. and K.U.; formal analysis, E.L., J.H., and K.U.; investigation, E.L., J.H., K.U., S.M. and U.P.; resources, A.W., C.B., F.K., H.Z., M.C. and P.M.; data curation, E.L., J.H., S.M., K.U. and U.P.; writing—original draft preparation, E.L., G.L., J.H. and K.U.; writing—review and editing, C.B., C.K., F.K., G.L., K.L., M.R. and S.M.; visualization, E.L., J.H. and K.U.; supervision, C.B., C.K., G.L., M.R. and K.U.; project administration, G.L. and K.U.; funding acquisition, C.B., H.Z. All authors have read and agreed to the published version of the manuscript.

Conflict of interest statement

The authors declare that they have no known competing financial interests or personal relationships that could have appeared to influence the work reported in this paper.

Acknowledgments

The authors want to thank S. Heuer, L. Holler and C. Innerlohinger for their excellent technical assistance; all co-workers of the Clinical Cooperation Group "Personalized Radiotherapy in Head and Neck Cancer" for scientific support.

Appendix A. Supplementary data

Supplementary data to this article can be found online at https://doi.org/10.1016/j.ejca.2022.08.033.

References

[1] Hess J, Unger K, Maihoefer C, Schuttrumpf L, Wintergerst L, Heider T, et al. A five-MicroRNA signature predicts survival and disease control of patients with head and neck cancer negative for HPV Infection. Clin Cancer Res 2019;25:1505–16.
[2] Tran KA, Kondrashova O, Bradley A, Williams ED, Pearson JV, Waddell N. Deep learning in cancer diagnosis, prognosis and treatment selection. Genome Med 2021;13:152.
[3] Lopez-Garcia G, Jerez JM, Franco L, Veredas FJ. Transfer learning with convolutional neural networks for cancer survival prediction using gene-expression data. PLoS One 2020;15: e0230536.
[4] Cancer Genome Atlas N. Comprehensive genomic characterization of head and neck squamous cell carcinomas. Nature 2015; 517:576–82.
[5] O'Sullivan B, Huang SH, Su J, Garden AS, Sturgis EM, Dahlstrom K, et al. Development and validation of a staging system for HPV-related oropharyngeal cancer by the International Collaboration on Oropharyngeal cancer Network for Staging (ICON-S): a multicentre cohort study. Lancet Oncol 2016;17:440–51.
[6] Alsahafi E, Begg K, Amelio I, Raulf N, Lucarelli P, Sauter T, et al. Clinical update on head and neck cancer: molecular biology and ongoing challenges. Cell Death Dis 2019;10:540.
[7] Leemans CR, Snijders PJF, Brakenhoff RH. The molecular landscape of head and neck cancer. Nat Rev Cancer 2018;18: 269–82.
[8] Maihoefer C, Schuttrumpf L, Macht C, Pflugradt U, Hess J, Schneider L, et al. Postoperative (chemo) radiation in patients with squamous cell cancers of the head and neck - clinical results from the cohort of the clinical cooperation group "Personalized Radiotherapy in Head and Neck Cancer. Radiat Oncol 2018;13:123.
[9] Selvaraju RR, Cogswell M, Das A, Vedantam R, Parikh D, Batra D. Grad-CAM: visual explanations from deep networks via gradient-based localization. Int. J. Comput. Vision 2019;128: 336–59. https://doi.org/10.1007/s11263-019-01228-7.
[10] Cerami E, Gao J, Dogrusoz U, Gross BE, Sumer SO, Aksoy BA, et al. The cBio cancer genomics portal: an open platform for exploring multidimensional cancer genomics data. Cancer Discov 2012;2:401–4.
[11] Gao J, Aksoy BA, Dogrusoz U, Dresdner G, Gross B, Sumer SO, et al. Integrative analysis of complex cancer genomics and clinical profiles using the cBioPortal. Sci Signal 2013;6:pl1.
[12] Wintergerst L, Selmansberger M, Maihoefer C, Schuttrumpf L, Walch A, Wilke C, et al. A prognostic mRNA expression signature of four 16q24.3 genes in radio(chemo)therapy-treated head and neck squamous cell carcinoma (HNSCC). Mol Oncol 2018; 12:2085–101.
[13] Liberzon A, Birger C, Thorvaldsdottir H, Ghandi M, Mesirov JP, Tamayo P. The Molecular Signatures Database (MSigDB) hallmark gene set collection. Cell Syst 2015;1:417–25.
[14] LeCun Y, Bengio Y, Hinton G. Deep learning. Nature 2015;521: 436–44.
[15] Krizhevsky A, Sutskever I, Hinton GE. ImageNet classification with deep convolutional neural networks. Adv Neural Inf Process Syst 2012;25.
[16] Kingma DP, Ba J. Adam: a method for stochastic optimization. arXiv:14126980 2017. https://doi.org/10.48550/arXiv.1412.6980.

[18] Adebayo J, Gilmer J, Muelly M, Goodfellow I, Hardt M, Kim B. Sanity checks for saliency maps. arXiv:1810.03292 2018. https://doi.org/10.48550/arXiv.1810.03292.

[19] Hanley JA, McNeil BJ. The meaning and use of the area under a receiver operating characteristic (ROC) curve. Radiology 1982;143:29–36.

[20] Saito T, Rehmsmeier M. The precision-recall plot is more informative than the ROC plot when evaluating binary classifiers on imbalanced datasets. PLoS One 2015;10:e0118432.

[21] Martinez I, Wang J, Hobson KF, Ferris RL, Khan SA. Identification of differentially expressed genes in HPV-positive and HPV-negative oropharyngeal squamous cell carcinomas. Eur J Cancer 2007;43:415–32.

[22] Wang HF, Wang SS, Tang YJ, Chen Y, Zheng M, Tang YL, et al. The Double-Edged Sword-how human Papillomaviruses Interact with Immunity in head and neck cancer. Front Immunol 2019;10:653.

[23] Worsham MJ, Ali H, Dragovic J, Schweitzer VP. Molecular characterization of head and neck cancer: how close to personalized targeted therapy? Mol Diagn Ther 2012;16:209–22.

[24] Baumeister P, Zhou J, Canis M, Gires O. Epithelial-to-mesenchymal transition-derived heterogeneity in head and neck squamous cell carcinomas. Cancers (Basel). 2021;13.

[25] Kim SW, Cheon K, Kim CH, Yoon JH, Hawke DH, Kobayashi R, et al. Proteomics-based identification of proteins secreted in apical surface fluid of squamous metaplastic human tracheobronchial epithelial cells cultured by three-dimensional organotypic air-liquid interface method. Cancer Res 2007;67:6565–73.

[26] Chang CW, Chen YS, Chou SH, Han CL, Chen YJ, Yang CC, et al. Distinct subpopulations of head and neck cancer cells with different levels of intracellular reactive oxygen species exhibit diverse stemness, proliferation, and chemosensitivity. Cancer Res 2014;74:6291–305.